THE ASTROPHYSICAL JOURNAL, 325:864–879, 1988 February 15

TWO LINES OF SIGHT WITH EXCEEDINGLY ANOMALOUS ULTRAVIOLET INTERSTELLAR EXTINCTION

JASON A. CARDELLI[1] AND BLAIR D. SAVAGE[1]
Washburn Observatory, University of Wisconsin-Madison
Received 1987 May 15; accepted 1987 August 12

ABSTRACT

Low-resolution *IUE* data obtained toward HD 62542, a B5 V star in a line of sight associated with a dark cloud in the Gum nebula region near ζ Pup (O5 Iaf) and γ Vel (WC8 + O9 I), yield an extinction curve with an extremely broad and weak UV extinction bump and the highest far-UV extinction yet observed in the Milky Way, reaching a value of $E(1200-V)/E(B-V) \approx 15$. The weak bump is very similar to the bump observed toward HD 29647, a highly reddened late B HgMn star in the Taurus dark cloud. Using HgMn comparison stars, we have derived a new curve for HD 29647 which we believe accurately represents the extinction in this line of sight. The far-UV extinction toward HD 29647 is larger than normal but not as extreme as that observed for HD 62542.

Using analytic fitting techniques, we have derived parameters which describe the central position and FWHM for the weak bumps observed toward HD 62542 and HD 29647. In both cases, the bump central positions are shifted shortward of 2175 Å with $\lambda_0 = 2110$ Å for HD 62542 and $\lambda_0 = 2128$ Å for HD 29647. For HD 62542 and HD 29647, we find the bump FWHM to be 1.29 μm^{-1} and 1.62 μm^{-1}, respectively, as compared with 0.992 μm^{-1} for the average of the stars as reported by Fitzpatrick and Massa (1986). These two lines of sight provide the most extreme examples of anomalous UV bump extinction yet observed and reveal that there are occasionally substantial changes in the position and width of the bump which may be produced by environmental factors.

The dense region that gives rise to the extinction observed toward HD 62542 is exposed to both intense UV radiation and stellar winds from ζ Pup and the γ Vel system. Strong shocks are undoubtedly exerting influence on the grains in this region. In contrast, the region responsible for the observed extinction toward HD 29647 is representative of a typical cold and quiescent molecular dark cloud. There is no evidence of any shocks in this line of sight. The similarity of the observed UV extinction bumps in these two regions coupled with their extreme positions and widths and highly contrasted environments provide important new hints to the origin of the material responsible for the 2175 Å bump. The extreme nature of the far-UV extinction observed toward HD 62542 may also help to constrain the range of possible explanations of the far-UV rise in interstellar extinction.

Subject headings: interstellar: matter — spectrophotometry — ultraviolet: spectra

I. INTRODUCTION

The ubiquitous 2175 Å interstellar extinction feature is by far the strongest known interstellar spectroscopic feature. For lines of sight with normal interstellar extinction (e.g., Seaton 1979, Savage and Mathis 1979) and $E(B-V) = 1$, the 2175 Å interstellar extinction feature or bump as it is frequently called has an equivalent width of ~ 1000 Å. By comparison, the same line of sight will typically have a neutral hydrogen column density of $\sim 5 \times 10^{21}$ atoms cm^{-2} which will produce an H I Lyα line having an equivalent width of ~ 50 Å. Among other potential dust features, the strongest measurable diffuse interstellar bands are typically less than 2 Å (Herbig 1975). The origin of the 2175 Å feature must rank as one of the most important unsolved spectroscopic problems involving the interstellar medium.

Recently, serious attempts have been made to measure reliably the properties of the 2175 Å feature in diffuse and dark cloud lines of sight through a parameterization of the bump's strength, shape, and position (Massa and Fitzpatrick 1986; and Fitzpatrick and Massa 1986). Fitzpatrick and Massa (1986) fitted the bump profiles for extinction along 45 lines of sight including a number exhibiting peculiar extinction (e.g., Her 36 and θ Ori). Their results indicate that the bump position is very stable with an extreme deviation from 2175 Å of only ± 17 Å. However, the bump width (i.e., FWHM) shows large variations of anywhere from 0.77 μm^{-1} (360 Å) to 1.25 μm^{-1} (600 Å) and the bump strength normalized to $E(B-V)$ also shows large variability. The bump width seems to correlate roughly with crude indicators of line-of-sight dust density as measured by $E(B-V)/r$, where r is the distance to the reddened star. As discussed by Savage (1975), the very restricted range in variation of the bump position places very severe constraints on the possible range of parameters of the particles responsible for the feature. For recent discussions of this problem see Hecht (1986) and Mathis (1987).

While the centroid of the 2175 Å absorption feature for dust in the diffuse interstellar medium seems remarkably constant, it is noteworthy that several objects with *circumstellar* dust exhibit broad ultraviolet absorption features at wavelengths significantly different than 2175 Å. A 2400 Å absorption feature is seen toward R CrB stars and the carbon-rich planetary nebula Abell 30 (Hecht *et al.* 1984; Greenstein 1981). Some of the B and early A stars with circumstellar dust studied by

[1] Guest Observers with the *International Ultraviolet Explorer* satellite which is sponsored and operated by the National Aeronautics and Space Administration, the Science Research Council of the United Kingdom, and the European Space Agency.

Sitko, Savage, and Meade (1981) have extinction in the middle ultraviolet for which the 2175 Å bump is either weak or missing entirely and the underlying extinction often contains shoulders or slope changes in the region 2500 Å and 2000 Å (see Hecht and Nuth 1982 for additional discussions of these objects). Unfortunately, a serious complication in interpreting many of the ultraviolet circumstellar dust measurements is the presence of absorption from the circumstellar gas which can be confused with absorption by the dust.

In order to probe the extreme range of fundamental properties of the 2175 Å feature, we have initiated an observing program with the *International Ultraviolet Explorer* (*IUE*) satellite to obtain measures of ultraviolet extinction toward stars known through broad-band UV photometry to have highly abnormal UV extinction. The object selection is based on the catalog of UV extinction measures provided by *ANS* satellite UV photometry (Savage *et al.*1985). The results for one of the objects we observed (HD 62542) are so interesting that we are reporting on the data here separately. Furthermore, the nature of the extinction bump in this line-of-sight is very similar to the feature observed toward HD 29647 which was presented in preliminary form by Snow and Seab (1980). We are therefore including a reevaluation of that curve here. Finally, we have undertaken an analysis of the properties of these two extremely peculiar extinction curves utilizing the parameterization scheme of Fitzpatrick and Massa (1986) and discuss the results in context with theirs and the environments in which these interesting lines-of-sight reside.

II. OBSERVATIONS AND REDUCTIONS

The observed objects are listed in Table 1. The UV data for HD 62542 were obtained by us. The remaining UV data were obtained from the *IUE* archives. The sources for the photometry and spectral classification are also listed. All of the UV data were reduced at the Midwest Astronomical Data Reduction and Analysis Facility (MADRAF) at the University of Wisconsin, Madison. With the exception of HD 62542, all of the long-wavelength data were obtained with the LWR camera. In order to standardize the observations, all LWR images were corrected for LWR sensitivity degradation using the results of Clavel, Gilmozzi, and Prieto (1986). No such correction is currently available for the LWP camera. Also, little information is available on the uncertainty associated with comparing LWP and LWR images. Clayton and Fitzpatrick (1987) have compared observations of a few stars obtained with both the LWP and LWR cameras and find no significant systematic differences between the two cameras. However, Harris and Cassatella (1985) have shown that apparent problems in the intensity transfer function (ITF) seem to result in systematically higher fluxes in the LWP camera at the overlap with the SWP camera for *weak* exposures. The shift in the spectrum appears to be confined to the region 1900 Å–2100 Å. For reasonably exposed spectra (data number = DN $\geq$ 130) the shift appears to be less than 10%. For our three LWP images of HD 62542, the exposure at 2100 Å ranged from 130 to 180 DN (camera saturation occurs at 255 DN). We feel that any systematic errors in our combined LWP data are less than 10% (see Fig. 1) and probably only affected the region below 2100 Å. Recent tests comparing a new LWP ITF (Cassatella and Lloyd 1987) with the one used with our data indicate that a decrease in the flux below 2200 Å of order 3%–5% relative to the region $\lambda > 2300$ Å occurs if the new ITF is used. We shall discuss the implications of this in § IV*a*.

a) HD 62542

The reduced flux data for HD 62542 are shown in Figure 1. Also shown are the data for the two B5 V comparison stars, 23 Cyg and ρ Aur, listed in Table 1. The spectrum of HD 62542

TABLE 1

REDDENED AND COMPARISON STARS

Name	V	$B-V$	Sp Type	References	*IUE* Images	Aperture	Exp.(s)
HD 62542	8.04	0.17	B5 V	1	SWP 28644	L	145
					SWP 29212	L	300
					SWP 29213	L	600
					LWP 8580	L	140
						S	130
					LWP 9077	L	60
					LWP 9078	L	240
HD 34759 ρ Aur	5.22	−0.15	B5 V	2, 3, 4	SWP 15537	L	8.6
					LWR 9868	L	7.7
HD 188665 23 Cyg	5.14	−0.13	B5 V	2, 3, 4	SWP 15338	L	5.4
					SWP 15339	L	8.0
					LWR 11856	L	8.2
					LWR 12008	L	9.2
HD 29647	8.37	0.90	B8 IV–IIIp	1	SWP 6557	L	10800
					LWR 5641	L	7200
					LWR 8532	L	900
HD 78316 κ Cnc	5.23	−0.11	B7–8 IIIp	5, 6, 7	SWP 15804	L	24
					SWP 15820	L	24
					LWR 12175	L	15
					LWR 12184	L	15
HD 144206 υ Her	4.76	−0.11	B9 IIIp	5, 6, 8	SWP 4965	L	7
					LWR 4297	L	4

REFERENCES.—(1) See text. (2) Wu *et al.* 1983 standard star. (3) Lesh 1968. (4) Eggen 1969. (5) Leckrone 1973, and references therein. (6) Cowley *et al.* 1969; Jashek *et al.* 1980. (7) HgMn stars; Leckrone 1973. (8) Johnson 1966; Jashchek *et al.* 1980.

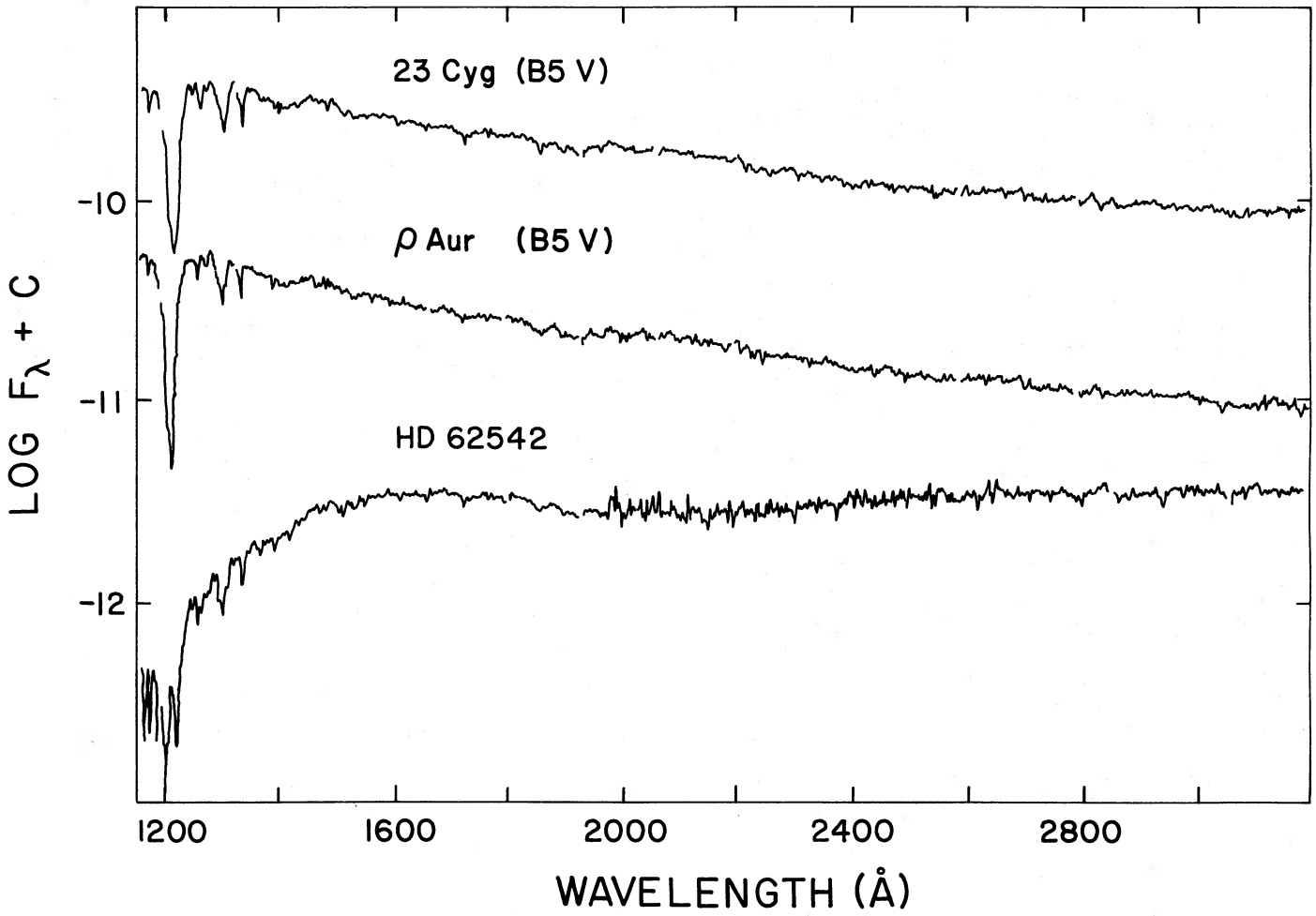

FIG. 1.—Logarithm of the *IUE* flux (in ergs cm^{-2} s^{-1} $Å^{-1}$) data of HD 62542. Also plotted are the data for the two B5 V comparison stars listed in Table 1. The gaps in the spectra correspond to the removal of reseaux and hot pixels from the data. The absolute flux for each object can be retrieved by adding a constant, C, to the scale shown on the figure. The constants for 23 Cyg, ρ Aur, and HD 62542 are $C = 0$, 1.0, and 0, respectively.

was constructed by splicing together the individual observations listed in Table 1. These observations included both normal and heavily exposed images which were necessary in order to obtain an improved signal-to-noise ratio (S/N) in the region of the bump as well as for $\lambda < 1600$ Å. For the combined spectra for each camera, the saturated portions were removed and the individual images were binned together. Finally, the combined SWP and LWP images were spliced together in the overlap region 1900–2000 Å. The only apparent discrepancy in the fit occurs in the region 1900 Å–1950 Å where the combined LWP data appear to be about 5%–10% higher than the SWP data. We subsequently gave the SWP data higher weight in this region when we combined the two images.

The V and $B-V$ photometry for HD 62542 is from Cousins, Eggen, and Stoy (1961) and Cousins and Stoy (1962). The B5 V spectral classification comes from Feast, Thackeray, and Wesselink (1955), Cousins and Stoy (1962), and Cousins, Eggen, and Stoy (1961). No peculiarities are noted in any of the sources which would lead one to question the spectral class assignment. Unfortunately, no $U-B$ color is available. However, Cousins, Eggen, and Stoy (1961) did determine a $(U-B)_c$ color (measured on the Cape Observatory system). Although the two systems are generally not transformable, a crude transformation was constructed using a large number of reddened and unredded B0–A0 stars found in the references quoted above. The quoted $(U-B)_c$ color corresponded to a range of reddened $U-B$ colors (using $B-V = 0.17$) appropriate for spectral types B4 V to B6 V.

The UV spectrum of HD 62542 was placed on a grid of UV comparison stars obtained from the *IUE* Atlas of Wu *et al.* (1983) in order to obtain the best UV spectral match. The grid ranged from B1 V to B9 V and included type III stars as well. The stellar features used for comparison included Si II (λ1260), Si III (λ1300), Si II (λ1306), C II (λ1334), Si IV (λ1400), and the luminosity-sensitive Fe III features at λ1900. For a complete discussion on the behavior of these features with temperature and gravity, see Panek and Savage (1976) and Koornneef and Code (1981). Types earlier than B3 were eliminated due to moderate to strong ($\geq$10%) mismatch for nearly all of the spectral lines, especially Si II (λ1260) and Si III (λ1300). For type B6, the Si II lines (λ1260, λ1306) are noticeably stronger and grow rapidly for later types (40% stronger than the lines seen in HD 62542 by type B7). For types B3–B5, no significant differences in the spectral line strengths longward of Lyα are apparent at the resolution of our data. There is some stellar absorption in the region 1190–1200 Å that rapidly increases in strength for types later than B3. From this, type B5 seems to

yield the most suitable comparison. However, the data in this region are weak and thus not extremely reliable and so we cannot totally discount types B3–B4 V on the basis of the UV observations.

In establishing a UV luminosity classification of HD 62542, we note that the Fe III features at 1900 Å are very luminosity sensitive and were sufficient to confine the luminosity class to the range III–V. For types B3–B5, the differences in the feature strengths between class III and V objects are relatively small and so we cannot be definitive about the luminosity class from the *IUE* data alone. However, based on the fact that all three of the optical classification spectrograms indicate class V, we feel that it is justifiable to exclude giants from the discussion.

b) HD 29647

Figure 2 displays the reduced flux data for HD 29647. The optical photometry in Table 1 was obtained from Crutcher (1985) and references therein. As with HD 62542, the data shown in Figure 2 are the result of combining the SWP and LWR images listed in Table 1. LWR 5641 was saturated in the region $\lambda > 2450$ Å in order to produce reasonable S/N around the bump (Snow and Seab 1980) and so the weaker spectrum LWR 8532 was fitted in the region 2400–2450 Å.

Straizys, Wisniewski, and Lebofsky (1982) and Straizys, Cernis, and Hayes (1985) report that HD 29647 shows abnormally strong Hg and Mn lines, placing it in the peculiar subclass of HgMn stars (for a good discussion see Wolff 1983, and references therein). Straizys, Cernis, and Hayes (1985) also give $\log g = 3.7$ indicative of class IV. Close examination of optical spectrophotometry obtained by one of us (J. A. C.) indicates that the Balmer jump is too large for a main-sequence star of the same temperature as inferred from the strength of the hydrogen Balmer lines. We estimate that the gravity is probably indicative of a late B giant. This is supported by Crutcher (1985) who indicates a luminosity of III–IV.

The optical line blanketing of HgMn stars is small (Wolff 1967), and consequently the optical continua of HgMn stars do not appear significantly different from normal stars of the same temperature. Hence, the $U-B$ and $B-V$ colors of HgMn stars do not appear to deviate from their normal star counterparts (Cameron 1966). However, there is evidence that the UV continua of HgMn stars deviate from their normal counterparts. Using *OAO 2* data, Leckrone (1973) analyzed a number of abundance-peculiar A and B stars in the UV, including a number of HgMn stars. He found that HgMn stars tend to be underluminous in the UV compared to normal stars of similar

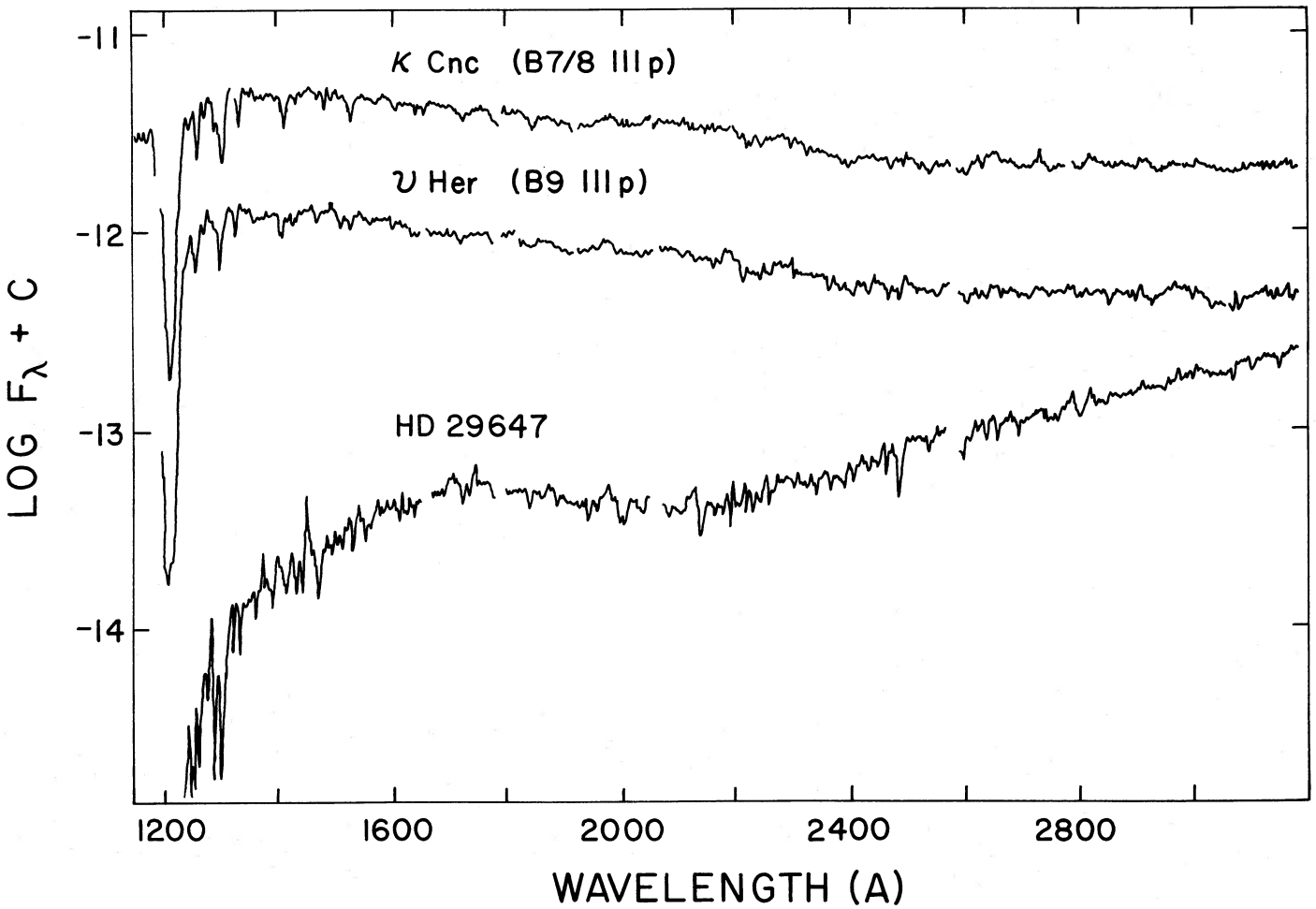

FIG. 2.—Logarithm of the *IUE* flux (in ergs cm^{-2} s^{-1} $Å^{-1}$) data of HD 29647. Also plotted are the data for the two HgMn comparison stars listed in Table 1. The gaps in the spectra correspond to the removal of reseaux and hot pixels from the data. The absolute flux for each object can be retrieved by adding a constant, C, to the scale shown on the figure. The constants for κ Cnc, υ Her, and HD 29647 are $C = 1.5$, 2.25, and 0, respectively.

temperature. Depending on the temperature, the differences range from 0.3 to 0.5 mag in the region 1400–2400 Å and are wavelength dependent.

The treatment of HD 29647 and its subsequent peculiar extinction in the literature has generally been handled from the perspective of a normal late B main-sequence star. The primary extinction curve for HD 29647 derived by Snow and Seab (1980) used a class Ia comparison star which we consider to be inappropriate. The data we present provide complete coverage in the UV region (the Snow and Seab data had a gap in the region 2400–3100 Å due to *IUE* detector saturation). Finally, the type V comparison stars used by Snow and Seab (1980) were obtained from the TD1 data of Nandy *et al.* (1976). The known differences between the TD1 and *IUE* absolute calibrations (Bohlin *et al.* 1980) were apparently not allowed for in calculating the observed extinction curves. Also, based on the above luminosity classification discussions, comparison of HD 29647 to normal class V stars is inappropriate. We feel that the best comparison stars for HD 29647 should come from the HgMn subclass. Only a few such stars have been observed with *IUE*. Two such stars, κ Cnc and υ Her, are listed in Table 1 and appear in Figure 2. Placement of the *UBV* data of these two stars on a two-color diagram for class III stars (FitzGerald 1970) indicates that the $U-B$ and $B-V$ colors are essentially the same as those for unreddened normal stars. The spectrum of HD 29647 seems to indicate additional line absorption not seen in either HgMn comparison star. The nost notable differences occur at about 1470, 2000, 2140, and 2500 Å. The feature near 2500 Å may be produced by strong Mn II resonance lines. Even with these absorption line differences, we feel that from the limited UV work on these stars, the intrinsic continuum is best matched with HgMn stars of the appropriate temperature range.

III. EXTINCTION CURVES: DERIVATION AND UNCERTAINTY

The extinction curves presented here were derived by the standard pair method. Briefly, this involves comparing the colors $m(\lambda-V)$ of the reddened program star with the *dereddened* colors of a lightly reddened or unreddened comparison standard. The derived curves are then normalized by the color excess of the reddened program star. The comparison stars for HD 62542 were taken from Wu *et al.* (1983). For HD 29647, two late B HgMn stars were chosen from the *IUE* archives. Below, the derived extinction curves and possible uncertainties are discussed separately for each star.

a) HD 62542

The extinction curve derived for HD 62542 using a B5 V comparison star appears in Figure 3. The corresponding optical color excess is $E(B-V) = 0.33$. Also plotted is the average Milky Way extinction curve of Seaton (1979). The specific curve shown for HD 62542 was derived using ρ Aur because the intrinsic reddening for this standard is the smallest of the two comparison stars ($E[B-V] = 0.01$). However, the curve using 23 Cyg ($E[B-V] = 0.03$) is essentially the same (see below). The gap in the extinction curve at $\lambda^{-1} \approx 8.2\ \mu\text{m}^{-1}$ corresponds to the position of Lyα which was strongly contaminated due to the effects of geocoronal Lyα in the observation of HD 62542.

Considering the relatively small $E(B-V)$, the curve in Figure 3 is remarkably smooth. The maximum scatter in the normalized curve for $\lambda^{-1} > 5\ \mu\text{m}^{-1}$ is of the order of ± 0.25 mag which corresponds to a relative uncertainty in the flux ratio of less than 10%. No noticeable effects of absorption line mismatch appear above the noise, which implies the lines have been matched to better than 10%, a fact which confirms that our choice of comparison star is probably reliable. For $\lambda^{-1} < 5\ \mu\text{m}^{-1}$, the scatter is somewhat larger, being about ± 0.4 mag in the region where the LWP camera has a low sensitivity and about ± 0.3 mag elsewhere.

As pointed out in § II, spectral types B3–4 V cannot necessarily be ruled out on the basis of the UV spectral classification alone. The *relative* scatter discussed above also applies to extinction curves determined with B3 V comparison stars despite the fact that the normalized extinction curves are slightly different. However, we suspect that type B3 V might be inappropriate for the following reasons. For types B2 V–B5 V, the Balmer jump rapidly increases at a rate of nearly 10% per spectral class (Kurucz 1979; Jacoby, Hunter, and Christian 1984). Use of a B3 V comparison star results in a normalized curve that is about $+0.4$ mag above the average curve at $\lambda^{-1} = 3.2\ \mu\text{m}^{-1}$ and about $+0.5$ mag above the curve for HD 62542 shown in Figures 3. Although there is no reason to expect our normalized curve to match the average curve at the overlap with the optical, most extinction curves *including* those for peculiar lines of sight generally normalize at or below the average curve. Comparatively few *properly* normalized curves are found above the average curve at $\lambda^{-1} = 3.2\ \mu\text{m}^{-1}$ and to our knowledge none are more than 0.3 mag above. Although eliminating type B3 V on this account alone is admittedly uncertain, the effects we see are completely in keeping with a mismatch at the Balmer jump.

In order to fully understand the accuracy of the curve shown in Figure 3, one must consider all possible sources of uncertainty, both random and systematic. A complete discussion of the sources and magnitude of these errors are presented in detail in Massa, Savage, and Fitzpatrick (1983) and Massa and Fitzpatrick (1986). Random errors arise in general from uncertainties in the visual photometry and zero-point photometric errors inherent in calibrated *IUE* data. For the normalized curve shown in Figure 3, use of the propagation-of-errors analysis of Massa, Savage, and Fitzpatrick (1983) indicates that the random errors are of the order of ± 0.2 mag at $\lambda^{-1} = 3.2\ \mu\text{m}^{-1}$, ± 0.4 mag at $\lambda^{-1} = 6.5\ \mu\text{m}^{-1}$, and up to ± 0.7 mag at $\lambda^{-1} = 8\ \mu\text{m}^{-1}$. Across the entire UV curve, this corresponds to a relative uncertainty of only ± 0.5 mag. [We have assumed $\sigma(B-V) = 0.015$, $\sigma(V) = 0.015$, and the systematic shifts appropriate for the LWP camera to be similar to those discussed for the LWR camera, see Bohlin *et al.* 1980.]

The major sources of possible systematic errors in our derived curve include comparison star temperature mismatch, improper dereddening of the comparison star, and errors introduced through possible ITF errors in the LWP camera data. As discussed in § II, this latter source will be confined primarily to the region around 2000–2100 Å. For the moment we will ignore this effect.

Using the convention of Massa, Savage, and Fitzpatrick (1983), the errors introduced through improper dereddening of the comparison star have the form $[E(B-V)_c/E(B-V)] \times [k(\lambda-V)_c - k(\lambda-V)]$, where $E(B-V)_c$ and $E(B-V)$ are the color excesses of the comparison and program stars, respectively, $k(\lambda-V)_c$ is the normalized extinction curve appropriate for the comparison star, and $k(\lambda-V)$ is the assumed average extinction curve (see, e.g., Seaton 1979). For $E(B-V)_c = 0.04$ and $\Delta k(\lambda-V) = 1$, the error would be of the order of only 0.13 mag. Comparison of the curves derived by using 23 Cyg

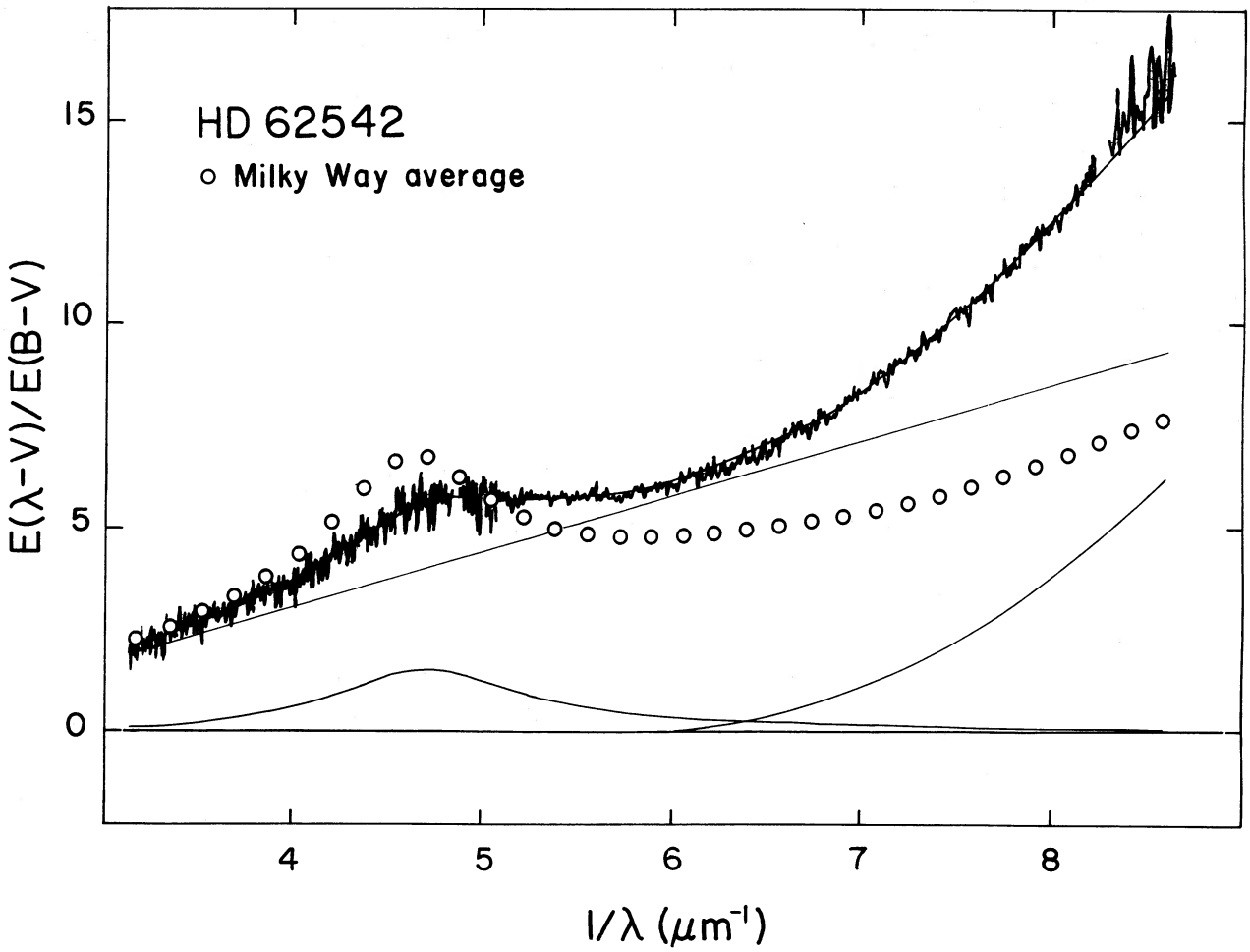

FIG. 3.—The normalized extinction curve determined for the line of sight to HD 62542 using the B5 V comparison star ρ Aur. The curve determined using the comparison star 23 Cyg (B5 V) is essentially identical as are the curves found using a B3 V and B4 V (see § III*a*). The open circles represent the average extinction curve of Seaton (1979). Also plotted are the three components that result from the fit procedure of Fitzpatrick and Massa (1986; see also § IV*a*) and the fit to the observed extinction.

($E[B-V]_c = 0.03$) and ρ Aur ($E[B-V]_c = 0.01$) shows that the two curves differ by less than ± 0.15 over the entire UV wavelength range. Given the low reddening of our comparison stars, we feel that the effect of this type of error in our curve will be less than 0.1 mag and is consequently of little importance.

Although we feel that B5 V is the best comparison star for HD 62542, as discussed in § II, we are unable to completely discount type B3–4 V. However, for early BV stars, the effect on a normalized extinction curve of mismatching by 1 to 2 spectral classes is generally small. This results from the fact that the analytic expression for the mismatch error is somewhat self-canceling in nature because it is proportional to the *ratio* of the terms $\Delta m(\lambda - V)$ and $E(B-V)$. Thus use of a hotter comparison star results in an increase in both $\Delta m(\lambda - V)$ and $E(B-V)$. For the extinction curve for HD 62542, we have examined mismatch errors empirically by comparing curves derived with both a B3 V and B4 V with the one shown in Figure 3 (B5 V). For the B3 V/B5 V case, $\Delta k(\lambda - V) = +0.5$ mag over the region $3.2\ \mu m^{-1} < \lambda^{-1} < 6.2\ \mu m^{-1}$. Beyond $\lambda^{-1} = 6.2\ \mu m^{-1}$, $\Delta k(\lambda - V)$ decreases monotonically to a value of $+0.25$ mag at $\lambda^{-1} = 8\ \mu m^{-1}$. For the B4 V/B5 V case, $\Delta k(\lambda - V)$ increases from $+0.3$ mag to $+0.4$ mag for $3.2\ \mu m^{-1} < \lambda^{-1} < 5.5\ \mu m^{-1}$ and decreases again monotonically to $+0.3$ mag at $\lambda^{-1} = 8\ \mu m^{-1}$. For both cases, $\Delta k(\lambda - V)$ shows negligible wavelength dependence for $\lambda^{-1} \leq 6\ \mu m^{-1}$. As discussed in the beginning of § III, these apparent zero-point shifts are totally in keeping with mismatch at the Balmer jump. Across the entire curve, the relative error due to mismatch in the worst case discussed here is less than 0.3 mag.

Collecting the errors discussed above and noting that their contributions are independent of each other, we find that the mean error relative to $\lambda^{-1} = 3.2\ \mu m^{-1}$ for the curve shown in Figure 3 is of the order of ± 0.3 mag.

b) HD 29647

The extinction curve derived for HD 29647 appears in Figure 4. Also plotted is the average curve of Seaton (1979). The comparison star used was υ Her although the curve derived using κ Cnc is essentially identical. The data for $\lambda^{-1} \geq 8\ \mu m^{-1}$ are very noisy and have been eliminated. Overall, the scatter in the curve is quite small with the exception of those features described in § II that showed no counterpart in either comparison star. Compared to the limited curve derived by Snow and Seab (1980), the scatter seen in Figure 4 is noticeably less. We feel that this is in part due to the better spectral match obtained by using HgMn comparison stars.

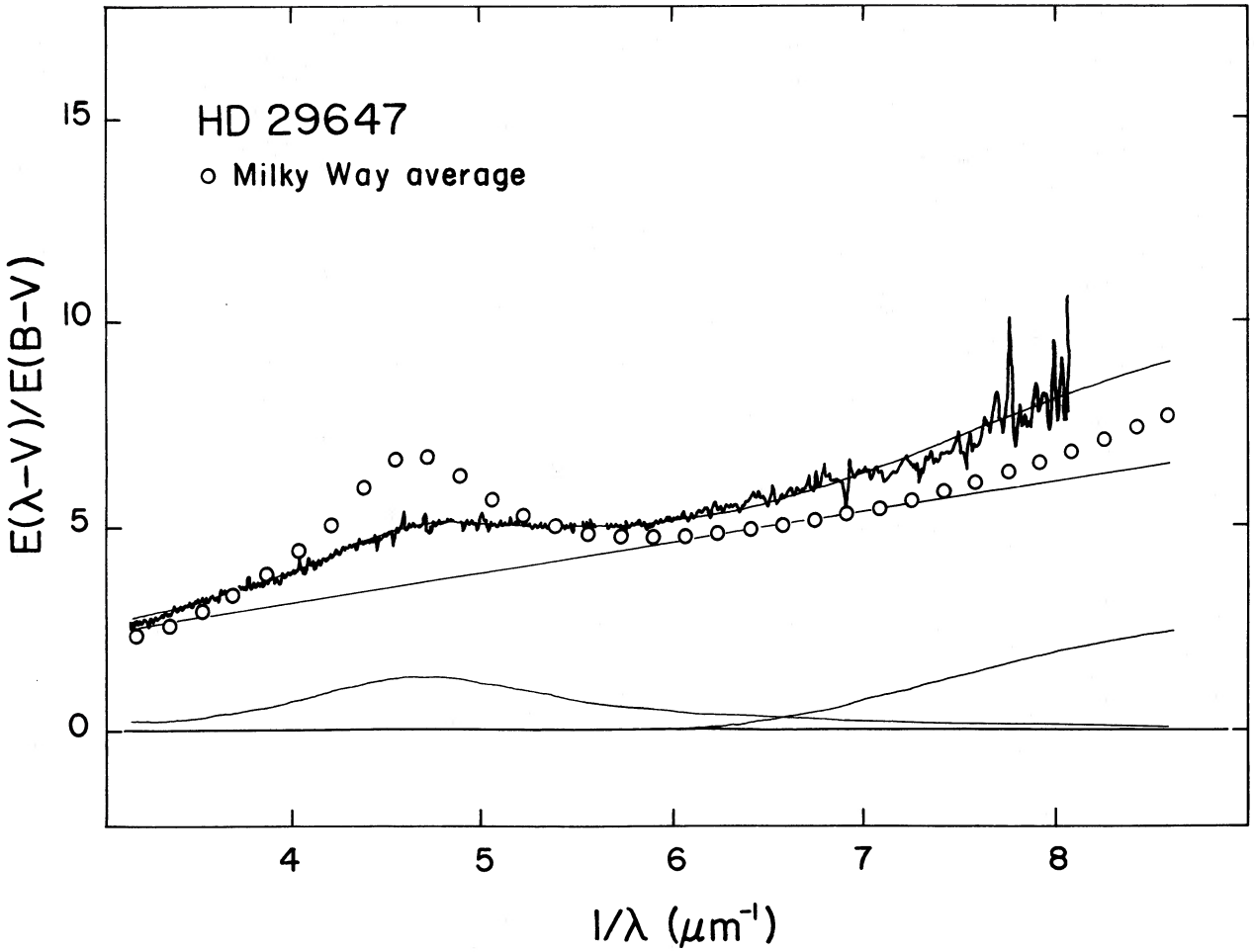

FIG. 4.—The normalized extinction curve determined for the line of sight to HD 29647 using the HgMn comparison star ν Her (B9 IIIp). The curve determined using the HgMn comparison star κ Cnc (B7/8 IIIp) is essentially identical (see § III*a*). The open circles represent the average extinction curve of Seaton (1979). Also plotted are the three components that result from the fit procedure of Fitzpatrick and Massa (1986; see also § IV*a*) and the fit to the observed extinction.

As can be seen in Figure 4, the normalized curve has a value that is +0.3 mag above the average curve at $\lambda^{-1} = 3.2\ \mu m^{-1}$. This shift is not due to mismatch at the Balmer jump, but represents the true position of the curve. This is confirmed by examining the broad-band optical extinction curve of HD 29647 determined by Straizys, Wisniewski, and Lebofsky (1982) which has a value that is +0.3 mag above the average curve at $\lambda^{-1} = 2.9\ \mu m^{-1}$. An optical extinction curve derived from 10 Å resolution spectrophotometry obtained by one of us (J. A. C.) yields a curve that is +0.25 mag above the average curve at $\lambda^{-1} \approx 3.1\ \mu m^{-1}$.

As with the curve for HD 62542, we estimate random errors using the propagation-of-errors analysis of Massa, Savage, and Fitzpatrick (1983). We find that these errors range from ± 0.06 mag at $\lambda^{-1} = 3.2\ \mu m^{-1}$ to ± 0.2 mag at $\lambda^{-1} = 8\ \mu m^{-1}$ corresponding to a relative uncertainty of less than ± 0.15 mag. Considering the size of the color excess toward HD 29647, $E(B-V) = 1.01$, it is not surprising that the errors are this small. A similar situation also applies to the errors corresponding to improper dereddening of the comparison star and spectral mismatch. In the case of the former, we have assumed $E(B-V) = 0$ for both HgMn comparison stars in our derivation of the extinction curve based on the discussion of the colors of HgMn stars in § II*b* and so no reddening correction was applied to the comparison stars. If the colors for these stars are in fact peculiar and $E(B-V) \neq 0$, then from the two-color diagram we require that the amount by which both $U-B$ and $B-V$ deviate from normal colors be exactly balanced by the effects of reddening. However, we find such a situation to be unlikely. Thus, if the colors are indeed normal and there is any reddening, it is probably hidden in the uncertainty of the optical photometry and is consequently of the order of $E(B-V) = 0.015$. In this context, an upper limit to this error can be found by considering the effect of *not* correcting for reddening at all. From this it follows that the relative error across the UV will be at most 0.06 mag. Even if $E(B-V) = 0.03$, the effect is still rather small and consequently of little relative importance.

Because of its peculiar nature, assessment of spectral mismatch errors for HD 29647 is somewhat more difficult than for normal stars. Examination of the data of Leckrone (1973) seems to indicate that HgMn stars show no more variance in their UV flux distributions from object to object than do normal stars of the same temperature. However, these data represent only a limited sampling of wavelengths in the UV, and unfortunately, the two HgMn stars listed in Table 1 represent the only existing high-quality low-resolution *IUE* data of this subclass of objects with the appropriate temperature. As

stated above, both comparison stars yield essentially the same curve within the random errors. We therefore have taken the approach of examining variances incurred if normal stars of similar temperature are used. Since we know that use of normal type V stars is certainly incorrect, such a procedure establishes a suitable worst case error estimate. For this purpose we have chosen to compare the differences, $\Delta k(\lambda - V)$, between the curve in Figure 4 and those derived by using B7 V, B8 V, and B8 III comparison stars. For both the B7 V and B8 V curves, $\Delta k(\lambda - V) \approx +0.2$ mag for $3.2\ \mu m^{-1} < \lambda^{-1} < 5\ \mu m^{-1}$. For $\lambda^{-1} > 5\ \mu m^{-1}$, $\Delta k(\lambda - V)$ rises steadily to a value of $+0.6$ mag at $\lambda^{-1} = 8\ \mu m^{-1}$. Because HD 29647 is luminosity class IV–III, this initial shift of $+0.2$ mag at the overlap with the optical is in keeping with a mismatch at the Balmer jump. This effect is clearly seen in the optical extinction curve when type B7 V or B8 V comparison stars are used. For the comparison with a B8 III, $\Delta k(\lambda - V) \approx 0$ for $3.2\ \mu m^{-1} < \lambda^{-1} < 4\ \mu m^{-1}$, which supports the Balmer jump mismatch for the type V curves discussed above. For $\lambda^{-1} > 4\ \mu m^{-1}$, $\Delta k(\lambda - V)$ decreases rapidly to -0.1 mag and stays constant until around $\lambda^{-1} = 8\ \mu m^{-1}$ where $\Delta k(\lambda - V) \approx -0.15$.

From the above discussion, we estimate the mean errors for the curve shown in Figure 4 are less than ± 0.2 mag and are probably dominated by the random errors. It appears that using a normal comparison star of type B8 III does not significantly affect the shape of the curve. It would seem that the most serious source of mismatch arises from using stars of the wrong luminosity class. We feel that the curve in Figure 4 is well determined and thus represents an accurate assessment of the extinction toward this line of sight.

IV. EXTINCTION CURVES: PARAMETERIZATION

From examination of Figures 3 and 4 it is easy to see that the normalized extinction toward these two lines of sight is quite peculiar, particularly in the region of 2175 Å. In order to understand the properties of the dust in these two regions, it is helpful to analytically quantify the properties of their extinction curves, particularly in the region of the 2175 Å feature. To this end, we have chosen to use the analytic parameterization scheme developed by Fitzpatrick and Massa (1986). This procedure involves performing a least-squares fit to the observed extinction using a linear (in λ^{-1}) background, a bump "profile" function over the range $3.2\ \mu m^{-1} \leq \lambda^{-1} \leq 5.9\ \mu m^{-1}$, and a cubic function for $\lambda^{-1} > 5.9\ \mu m^{-1}$.

Savage (1975) showed, using *OAO 2* data, that a linear background plus Lorentzian profile yields a good fit to the observed shape of the extinction bump. Seaton (1979) verified this result using *Copernicus* and *TD-1* satellite data. More recently, Massa and Fitzpatrick (1986) showed, using *IUE* observations of 33 stars in 5 open clusters, that such a procedure accurately codifies the shape of the extinction bump. Fitzpatrick and Massa (1986) have since performed parameterized fits for extinction observed in 45 lines of sight including a number exhibiting some of the most peculiar extinction observed in the Galaxy. However, they adopt a bump profile referred to as a Drude function which can be understood as an absorption cross section under the assumption of the Drude theory of metals (see Bohren and Huffman 1983). They find that in addition to being easier to physically interpret than a Lorentzian, the Drude function also yields slightly better fits. We have therefore adopted this approach, both for its validity and the fact that the results of Fitzpatrick and Massa (1986) supply a large data base to which our results can be reliably compared. The parameters determined from the bump fit include λ_0^{-1} and γ, the bump central position and width (i.e., FWHM), respectively, and are discussed below. The function used to fit the observed extinction is given in Table 2.

a) HD 62542

The extinction curve for HD 62542 clearly represents one of the most extreme examples of extinction yet observed in the Galaxy. In the region of the bump, the extinction appears rela-

TABLE 2

EXTINCTION BUMP PARAMETERS

Name	λ_0^{-1} (μm^{-1})	λ_0(Å)	γ (μm^{-1})	A (μm^{-1})	Comments
HD 62542	4.74	2110	1.29	3.11	1, 2
HD 29647	4.70	2128	1.62	3.35	3, 4
Average	4.599	2174	0.992	5.17	5, 45 star average
θ^1 C Ori	4.633	2158	0.835	2.43	5, λ_0^{-1} (max)
HD 38087	4.559	2193	1.000	6.68	5, λ_0^{-1} (min)
ζ Oph	4.579	2184	1.251	5.71	5, γ (max)
HD 93028	4.625	2162	0.786	2.62	5, γ (min)
30 Dor region	4.606	2171	0.894	2.62	6
LMC average	4.608	2170	0.994	4.03	6
Seaton curve	4.595	2176	1.051	5.92	6

NOTES.—Extinction curve fitting function:

$$\frac{E(\lambda - V)}{E(B - V)} = A_1 + A_2\lambda^{-1} + \frac{A_3}{[\lambda^{-1} - (\lambda_0^{-1})^2/\lambda^{-1}]^2 + \gamma^2} + A_4(\lambda^{-1} - 5.9)^2 + A_5(\lambda^{-1} - 5.9)^3 .$$

Also Note, for $\lambda^{-1} < 5.9\ \mu m^{-1}$, $A_4 = A_5 = 0$.

COMMENTS.—(1) Variances are $\sigma(\lambda_0^{-1}) = \pm 0.03$, $\sigma(\gamma) = \pm 0.04$, and $\sigma(A) = \pm 0.30$ and correspond to the observed range of parameters found using both B5 V comparison stars from Table 1. (2) Coefficients for the fitting function are $A_1 = -2.325$, $A_2 = 1.346$, $A_3 = 2.464$, $A_4 = 0.860$, $A_5 = -0.006$. (3) Variances are $\sigma(\lambda_0^{-1}) = \pm 0.01$, $\sigma(\gamma) = \pm 0.09$, and $\sigma(A) = \pm 0.25$ and correspond to the observed range of parameters found using both HgMn comparison stars from Table 1. (4) Coefficients for the fitting function are $A_1 = 0.358$, $A_2 = 0.725$, $A_3 = 3.975$, $A_4 = 0.783$, $A_5 = -0.168$. (5) These results from Fitzpatrick and Massa 1986 indicate the average bump parameter values and the most extreme deviations in λ_0^{-1} and γ among the objects in their sample. Both HD 62542 and HD 29647 have λ_0^{-1} and γ lying outside the range found by Fitzpatrick and Massa 1986. (6) Data from Fitzpatrick 1986.

tively broad and flat. In fact, if no prior knowledge of the shape of UV extinction is assumed, it is not clear that one would consider the region around 2200 Å in Figure 3 to be a bump at all. In other words, the bump region is so broad and flat that one has to question if a bump is even present in the traditional sense. It is possible that what is observed is the underlying nature of UV extinction in the absence of the bump.

One possible reason why the bump region appears as a broad plateau is the rather large amount of far-UV (FUV) extinction present in this line of sight. Although not exceedingly steep, the FUV reaches values that are larger than for any curve so far measured in the Milky Way. Compared to the Milky Way average of 6.4 mag, $E(1300-V)/E(B-V) = 12$ mag for HD 62542. By comparison, the value is 10 for the LMC 30 Dor region (Fitzpatrick 1986) while the value for the SMC is 14 (Prevot *et al.* 1984). For HD 62542, the extinction value at $\lambda^{-1} = 8.5\ \mu m^{-1}$ implies that the normalized extinction may reach 15 mag at the shortest wavelengths accessible to *IUE*.

Except for slope changes in the middle-UV, which could be interpreted as an extinction bump, the observed extinction curve in Figure 3 is featureless. We will assume for the moment that a bump is indeed present in the general region around 2200 Å. The results of the least-squares parameterization are shown in Figures 3 and 5*a*. In Figure 3, the fit to the extinction curve is overplotted on the observed curve. Also plotted are the individual components to the fit. As can be seen, the quality of the overall fit is good. In Figure 5*a*, the observed bump profile, found by subtracting the linear background and cubic FUV fit, is shown normalized to a peak value of 1 along with the determined Drude profile fit. As can be seen, the observed bump is fitted quite well. Also plotted for reference is the equivalent Drude function appropriate for the average interstellar curve of Seaton (1979).

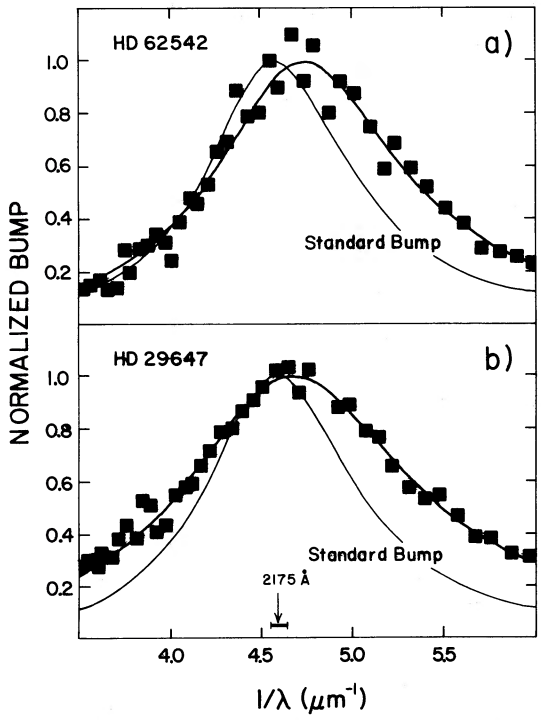

FIG. 5.—The computed best-fit Drude profiles normalized to a peak value of unity for the extinction curves observed toward (*a*) HD 62542 and (*b*) HD 29647. The filled squares represent the observed bump profile (binned in 20 Å intervals), normalized to unity, found by subtracting the computed linear background and FUV extinction fits from the curves shown in Fig. 3 and 4. Also plotted is the Drude profile for the average interstellar curve (Seaton 1979) as well as the extreme range of λ_0^{-1} found by Fitzpatrick and Massa (1986) for 45 lines of sight including a number exhibiting very peculiar extinction.

Table 2 lists the results of the bump fit discussed above. The bump area, $A \equiv \pi A_3/2\gamma$ where A_3 is the bump normalization coefficient (see Table 2), is representative of the relative bump strength and is included for reference. Also listed are the extreme values of λ_0^{-1} and γ found by Fitzpatrick and Massa (1986) along with the average for the 45 lines of sight they studied. Fitzpatrick and Massa (1986) empirically examined errors for the various bump parameters per unit $E(B-V)$ that are expected for individual extinction curves. Because these errors were determined empirically from *IUE* data, they include the effects of random errors discussed in § II. Given that our fit shows no noticeable systematic errors, we have adopted their results as first-order uncertainties. From their Table 2 we find $\sigma(\lambda_0^{-1}) = \pm 0.02\ \mu m^{-1}$, $\sigma(\gamma) = \pm 0.06\ \mu m^{-1}$, and $\sigma(A) = \pm 0.45\ \mu m^{-1}$. The variances listed in our Table 2 were derived by determining the bump parameters using both B5 V comparison stars. As can be seen, these empirical uncertainties are essentially the same as those derived from Fitzpatrick and Massa (1986). We also examined the bump parameters that result if spectral types B3 V and B4 V are used to derive the extinction curve. In both cases, λ_0^{-1} and A were within the variances shown in Table 2. Gamma was approximately 10% larger than the mean value listed in the table. The only other potential effect on the bump parameters is the possible ITF problems in the LWP camera. As discussed in § II, the most serious effect is a systematically higher flux of order 5%–10% in the region 2000 Å–2100 Å. Decreasing the observed stellar flux by 10% in this region would increase the observed extinction by about 0.3 mag over the interval $4.76\ \mu m^{-1} < \lambda^{-1} < 5.00\ \mu m^{-1}$. Such an increase would serve to shift the bump central position slightly to even shorter wavelengths but would not seriously affect the other parameters.

Compared to the results of Fitzpatrick and Massa (1986), λ_0^{-1} and γ for the bump observed toward HD 62542 represent the most extreme values yet observed. In terms of wavelength, $\lambda_0 = 2110$ Å compared with $\lambda_0 = 2158$ Å (θ Ori), the most extreme value found by Fitzpatrick and Massa (1986). Because the bump that we observe has the same functional shape as those seen in other lines of sight, it is tempting to assume that it is caused by the same material. However, because its central position is so removed from the normal position of 2175 ± 17 Å, we must consider that it could arise from some underlying component that is normally hidden by the standard bump. Considering the general invariance of observed bumps, the existence of such an extreme case makes this a reasonable possibility to explore.

b) HD 29647

Since its discovery (Snow and Seab 1980), no extinction bump has been observed that is as weak as the one seen toward HD 29647. In fact, the extinction curve is often referred as being without a bump, although Figure 4 clearly indicates that a bumplike structure is present. In some respects, the curve in Figure 4 is quite similar to the one for HD 62542 shown in Figure 3. Both curves are characterized by weak bumps and FUV extinction that is higher than average. This general simi-

larity is one of the major motivating factors behind our reanalysis of the extinction toward HD 29647.

The results of the parameterization of the extinction curve for HD 29647 are shown in Figures 4 and 5*b*. As with the HD 62542 curve, the computed extinction curve fit is overplotted on the observed curve. Also shown are the three components to the fit. It should be noted that the portion of the curve for $\lambda^{-1} > 6\ \mu m^{-1}$ is not fitted well. There appears to be more structure than can be accounted for by the functional form shown in Table 2. Relative to the fit shown in Figure 4, the structure is in the form of ~ 0.3 mag of excess extinction for 6 $\mu m^{-1} < \lambda^{-1} < 7\ \mu m^{-1}$ and ~ 0.3 mag less extinction for 7 $\mu m^{-1} < \lambda^{-1} < 7.5\ \mu m^{-1}$. In Figure 5*b*, the observed bump is plotted along with the best-fit Drude profile and the Drude profile appropriate for the average curve of Seaton (1979). As with the bump for HD 62542, the bump observed toward HD 29647 is fitted well by the Drude function.

Table 2 lists the relevant bump parameters determined from the fit procedure. From Fitzpatrick and Massa (1986), we estimate the errors in the fit to be $\sigma(\lambda_0^{-1}) = \pm 0.01\ \mu m^{-1}$, $\sigma(\gamma) = \pm 0.02\ \mu m^{-1}$, and $\sigma(A) = \pm 0.15\ \mu m^{-1}$. The variances determined from using both HgMn stars appear in Table 2. With the exception of λ_0^{-1}, our empirically determined variances are considerably larger than those deduced from Fitzpatrick and Massa (1986). This is not surprising, however, considering how weak the observed bump actually is (see Fig. 4). In analogy to weak and broad spectral features, centroids are generally much easier to determine than the FWHM or the equivalent width. In such a case, slight variations in the placement of the continuum can have large effects on the equivalent width because of significant information in the wings of the feature.

Despite the larger errors, we consider the bump parameters for HD 29647 to be relatively well determined. We of course make this statement with some caution keeping in mind the peculiar nature of HD 29647. Because little information still exists on the UV behavior of HgMn stars, we cannot be totally sure that use of the comparison stars in Table 1 has not introduced systematic errors into our bump parameters. However, parameterization of the bump produced by using a normal B8 III yielded results consistent with those listed in Table 2. The reddening to this line of sight is so large that the effects produced by extinction appear to dominate over any uncertainties associated with the stars peculiar status. We therefore accept the values listed in Table 2 as representative of the true extinction bump observed toward HD 29647.

Like HD 62542, the bump parameters for HD 29647 appear to deviate significantly from any bump yet measured. Although the bump is not as shifted as the one observed toward HD 62542, λ_0 for the HD 29647 bump is still shifted shortward of the standard bump position by nearly 50 Å. More impressive is the FWHM which, in units of μm^{-1}, is 30% larger than the most extreme example (ζ Oph) found by Fitzpatrick and Massa (1986) and nearly 70% larger than the average. These values are so different from what is normally observed that it is again tempting to attribute the bump extinction toward HD 29647 as being due to a possible subcomponent which is observed only in the absence of the normal bump component. Clearly, such a situation implies special physical conditions which are generally not applicable to most observed lines of sight. In the following section, we explore this possibility for both the HD 62542 and HD 29647 lines of sight by examining the environments in which the peculiar dust extinction arises.

V. INTERSTELLAR ENVIRONMENTS OF HD 62542 AND HD 29647

The peculiar extinction bumps presented for HD 62542 and HD 29647 represent either a previously unobserved subcomponent, or simply extreme modification of the normal bump carrier. The derived parameters are so different than all previous observed bumps (including peculiar bumps) that the physical conditions in the regions in which the dust exists must be extremely rare. In this section, we examine the regions in which these lines of sight occur in order to explore any physical parameters that might be responsible for the observed extinction.

a) HD 62542

The line of sight to HD 62542 is in a region of the sky which places it in the direction of the Gum nebula complex. In Hα emission, the complex appears roughly circular with a diameter of about 36° (Sivan 1974) and is comprised of patches and filaments of emission consistent with the image of an expanding bubble-like nebula (Reynolds 1976*a*). The distance to the center of the nebula is estimated to be of the order of 400 pc (Brandt *et al.* 1971; Gott and Ostriker 1971) which translates to a diameter of roughly 250 pc. The origin of the complex remains a mystery although a number of scenarios have been proposed. These include a "fossil Strömgren sphere" produced by the Vela supernova remnant progenitor (Brandt *et al.* 1971), a normal H II region being currently ionized by embedded hot stars (Beuermann 1973; Wallerstein, Silk, and Jenkins 1980), a 10^6 yr old supernova remnant currently being heated by hot stars (Reynolds 1976*a*, *b*), and an expanding bubble created by ionization and winds from embedded OB stars (Weaver *et al.* 1977).

Regardless of its origins, the observed Hα emission appears to be consistent with ionization from two major sources, namely ζ Pup (O5 Iaf) and γ Vel (WC8 + O9 I) (Reynolds 1976*a*, *b*). It also appears that some energy may also be supplied by stellar winds in the form of shocked gas as indicated by measured values of [S II]/Hα (Chanot and Sivan 1983). The likely sources of these winds are the WC8 star γ^2 Vel which has a mass-loss rate of 7.4–11.6 $\times 10^{-5}\ M_\odot\ yr^{-1}$ and a terminal wind velocity of $V_\infty = 1600\ km\ s^{-1}$ (Abbott *et al.* 1986; van der Hucht, Cassinelli, and Williams 1986) and ζ Pup which has a mass-loss rate of 3–7 $\times 10^{-6}\ M_\odot\ yr^{-1}$ and a terminal wind velocity $V_\infty = 2700\ km\ s^{-1}$ (Olson and Castor 1981).

In projected angular distance, HD 62542 is located $\sim 10°$ west-southwest of the projected center of the nebula defined by the Hα emission and resides coincident with a ridge of dark matter. Assuming a normal value of total-to-selective extinction and adopting $M_v = -1.0$ (Johnson and Iriarte 1958) we estimate the distance to the star to be of the order of 400 pc which places it inside the expanding shell at about the same distance as ζ Pup and γ Vel. With respect to the sources supplying the energy to the complex, HD 62542 is located 4°.5 southwest of ζ Pup and 7° northwest of γ Vel which at 400 pc translates to tangential distances of 31 and 49 pc, respectively. A photograph of the region where HD 62542 resides is shown in Figure 6. The directions to ζ Pup and γ Vel are indicated in the figure. As can be seen, the eastern edge of the ridge is extremely well defined giving the impression that matter has been swept up from the direction of ζ Pup and γ Vel. Examination of the reddening of B stars located east of the ridge and to the southwest and northwest of ζ Pup and γ Vel, respectively, yields typical values of $E(B-V) \leq 0.05$ suggesting that

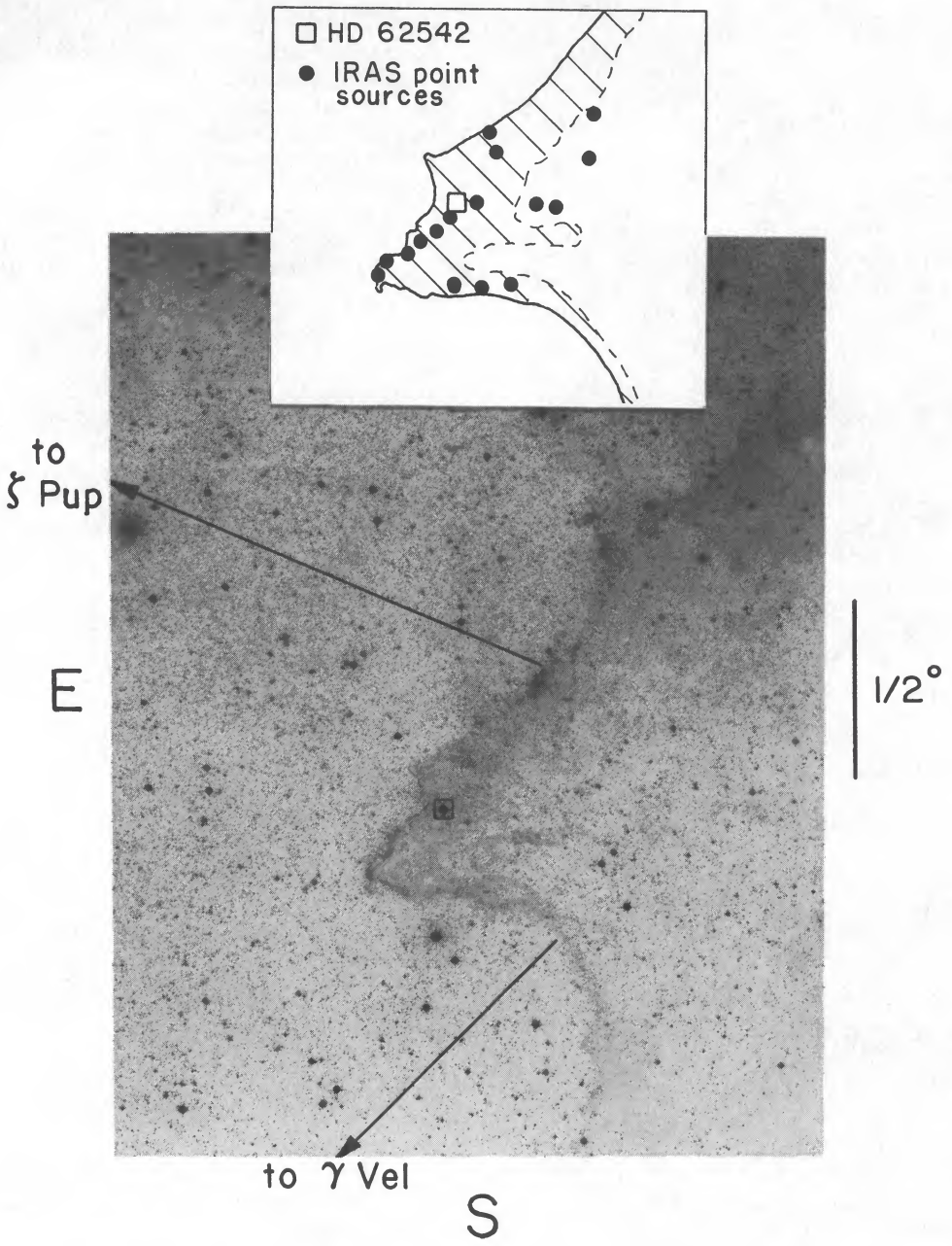

FIG. 6.—The environment through which the line of sight to HD 62542 passes. The directions to the nearby hot radiation/wind sources ζ Pup (O5 Iaf) and γ Vel (WC8 + O9 I) are also shown. The inset at the top shows (to scale) the observed distribution of dust as well as the position of HD 62542 (*open square*) and the distribution of observed *IRAS* point sources.

this is a cavity relatively void of dust and gas. This is confirmed by the Hα photograph of Sivan (1974) which shows this region void of emission. (This cavity is rimmed by relatively bright emission but it is difficult to determine if we are actually looking at a vacant volume surrounded by Hα emission or simply a hole in the foreground portion of the expanding shell.)

Superposition of the Hα photo on Figure 6 shows the ridge to be well defined by bright Hα emission with a relatively sharp cutoff at the eastern edge and more diffuse emission to the west. Faint emission is also visible in Figure 6. A major source of the photoionization is undoubtedly radiation from ζ Pup and possibly the O9 I companion of γ^2 Vel (Hua *et al.* 1983 report that the ionizing UV flux from WC8 stars would be negligible). It is quite plausible that shocks produced by winds from γ^2 Vel (1600 km s^{-1}) and ζ Pup (2700 km s^{-1}) are also producing some of the observed emission. The sharp eastern boundary, coupled with the ridge appearing bowed in regions of apparent lower density, also seems consistent with this picture. Interaction of strong winds with matter in this region is supported by the presence of numerous cometary-shaped dark globules to the southwest and northeast of the ridge, the tails of which point in the general direction of the wind flow from γ^2 Vel and ζ Pup. The easternmost portion of the ridge in which HD 62542 is located shows characteristics indicative of a cometary-like globule in formation. Figure 6 clearly shows this to be the densest portion of the ridge. To the north of HD

62542, the ridge appears to show the effects of turbulence which could be caused by shearing as the wind from γ^2 Vel flows along the edge of the dense material. Finally, the inset in Figure 6 shows the location of *IRAS* point sources observed in the 12 and 60 μm bands in the general direction of HD 62542. As can be seen, the majority of the point sources are coincident with the densest portion of the ridge. It is tempting to imagine that shocks might have triggered local collapse and possibly star formation. However, close examination of Figure 6 shows the matter in this part of the ridge to be rather clumpy and it is quite possible that what we are seeing are clumps of warm dust with peak emission in 60 μm band.

From the data of van der Hucht, Cassinelli, and Williams (1986), pressure balance between the wind from γ^2 Vel and the ambient medium will be achieved when $d^2nT = 7.8 \times 10^7$ pc^2 cm^{-3} K where d is the distance from γ^2 Vel in parsecs, n is the ambient density in cm^{-3}, and T is the ambient temperature. For nominal diffuse interstellar conditions ($T \approx 80$ K, $n \approx 20$ cm^{-3}), balance will be achieved for $d \approx 360$ pc. Of course, this estimate is an upper limit since it does not take into account the increase in density that would occur in front of the "snowplow" in the case of isothermal expansion. However, d will certainly be greater than 50 pc for the ambient conditions assumed above and so the wind could easily have evacuated the region to the east of the ridge. For pressure balance to occur at a distance $d \approx 50$ pc from γ^2 Vel, $nT \approx 3 \times 10^4$ cm^{-3} K. For a local gas temperature of 100 K, $n \approx 300$ cm^{-3} behind the ridge is sufficient to balance the wind. From this, we can conclude that the ridge seen in Figure 6 could easily remain well inside the Hα shell at a distance of 50 pc from γ^2 Vel. (We have used γ^2 Vel as an example because the mass flux produced by the wind is about a factor of 10 greater than that produced by ζ Pup. Inclusion of the wind from ζ Pup would not effectively alter the above discussion.)

If the ridge consists of a fair fraction of swept-up material from the cavity, then shock processing and sputtering will have had a profound effect on the observed grains. Some fraction of the observed grains may even have come from dust formed in the wind near the star. Even if material in the cavity has added little new matter to the ridge, shock heating as well as cloud compression must have modified the grains as seen by the extinction shown in Figure 3. This processing may include destruction as well as coagulation in the denser environments.

b) HD 29647

HD 29647 is a highly obscured late-B star in Taurus. With $E(B-V) = 1.01$, HD 29647 resides in a line of sight significantly more obscured than HD 62542 which has $E(B-V) = 0.33$. Crutcher (1985) has provided a comprehensive discussion of the properties of the region in which HD 29647 resides. It is situated within the area of Heiles cloud 2 and very close to the Taurus molecular cloud 1 (TMC 1), which is a very dense molecular clump within cloud 2. Crutcher's distance estimate for HD 29647 of 170 $\pm$ 20 pc suggests that the star lies beyond the Taurus dark cloud complex which lies at 140 $\pm$ 10 pc (Elias 1978). This view is supported by the appearance of the Palomar Sky Survey prints which show no indication of nebulosity which we would expect to see if HD 29647 were embedded in the dense interstellar region. In addition, the K and L photometric data of Straizys, Wisniewski, and Lebofsky (1982) show no evidence of infrared excess which is occasionally seen toward stars embedded in dense matter (e.g., ρ Oph). Finally, Crutcher (1985) finds that the column density derived from the optical CN absorption lines is in exact agreement with the column density derived from the millimeter CN emission lines which would occur only if the star was entirely behind the cloud.

The Palomar Sky Survey prints of the region around HD 29647 show no evidence of the very pronounced stellar-interstellar interaction which appears to be affecting the material in the line of sight to HD 62542 (see § V*a* and Fig. 6). Other indications of the quiescent nature of the HD 29647 line of sight come from the optical absorption line data of Crutcher (1985). Elitzur and Watson (1978, 1980) have proposed that CH^+ is formed in shock-heated gas via endothermic reactions of C^+ with H_2. Such a model has proved to be necessary because CH^+ is expected to be rapidily destroyed through reactions with electrons and H_2 and in many cases, the predicted ratio of $N(CH)/N(CH^+)$ through equilibrium chemistry yields values as much as two orders of magnitude larger than the observations (Federman 1982). For the line of sight to HD 29647, the data of Crutcher (1985) yield $N(CH)/N(CH^+) > 17$. For HD 147889, a star located in the ρ Ophiuchi dark cloud with a reddening similar to HD 29647, $N(CH)/N(CH^+) \approx 2.8$ (Cardelli and Wallerstein 1986). The radial velocities of the CH and CH^+ toward HD 147889 differ by 1.2 km s^{-1} which also conforms to shock formation theory (these results are also indicated for the general Ophiuchus complex; see Meyers *et al.* 1985). No such differences in velocity are found for the lines observed toward HD 29647. This, along with the large ratio of $N(CH)/N(CH^+)$, implies that shock production of CH^+ is negligible toward HD 29647. Thus, while shock processing may influence the extinction toward HD 62542 (unfortunately, no information is currently available on the optical absorption), the process probably does not play a role for the extinction observed toward HD 29647. The line of sight to HD 29647 suggests that the extinction is primarily produced in a relatively quiescent but very dense interstellar region. The diagnostic radio data of Crutcher (1985) reveal a region with very strong molecular lines and imply a high density of 800 cm^{-3} and a low kinetic temperature of 10 K, values typical of dark clouds.

VI. DISCUSSION

Figure 7 compares the extinction toward HD 62542 and HD 29647 with the average extinction in the Milky Way (from Seaton 1979), the Large Magellanic Cloud (LMC) and the 30 Doradus region of the LMC (both from Fitzpatrick 1986). The extinction curves for HD 62542 and HD 29647 are among the most anomalous so far observed for dust in diffuse or dense clouds. The sight lines to both objects exhibit extinction curves with middle ultraviolet extinction bumps which are very weak, very broad, and shifted in wavelength from the normal position of 2175 Å. In addition, both sight lines have larger than average FUV extinction with the curve for HD 62542 having the largest FUV extinction ever recorded for a Milky Way star. In fact this curve even exceeds the high FUV extinction seen toward the 30 Dor region in the LMC. The discussions of these two unusual extinction curves which follow will consider both the ultraviolet bumps and the FUV component of extinction.

a) The Extinction Bump

Observations providing new insights about the range of the spectroscopic behavior of the bump are potentially of great value to those experimental and theoretical studies which seek to determine the origin of the bump. The early measures of the

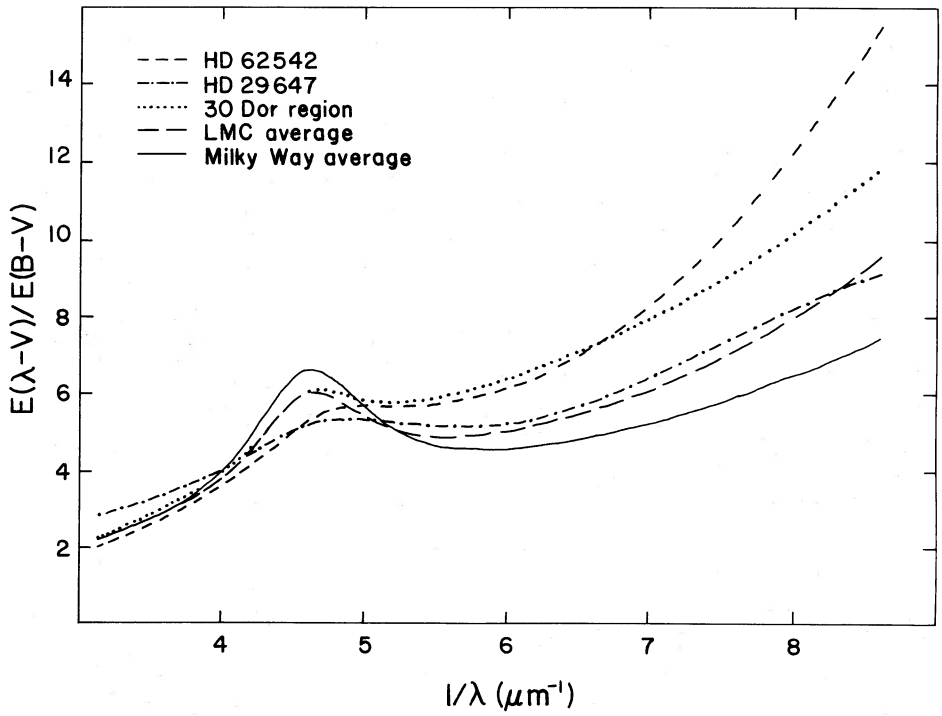

FIG. 7.—Comparison of the fit to the extinction curves observed toward HD 62542 and HD 29647 to the fits for the curve for the 30 Dor region, the LMC average curve, and the average Milky Way curve (Seaton 1979). These curves were generated from the fit parameters found in Fitzpatrick (1986).

extinction bump with the *OAO 2* satellite (Savage 1975) revealed a feature with a profile showing a remarkable degree of constancy among a sample of 36 stars. The observation that the bump position and shape were constant or very nearly constant placed severe restrictions on the grain geometrical parameters if the feature was explained by classical scattering theory employing bulk optical constants. In fact the restrictions seemed so severe that Savage (1975) suggested that alternative explanations may be required unless the grains which exist in widely separated regions of space and under very different physical conditions have nearly identical size and shape distributions. These restrictions can now be relaxed slightly because the *IUE* measurements reported by Fitzpatrick and Massa (1986) have revealed a 25% variation in the width of the ultraviolet extinction bump. However, for the Fitzpatrick and Massa sample of 45 extinction curves the bump exhibited an extreme position variation of only ± 17 Å or $\pm 0.8\%$. For a summary of the Fitzpatrick and Massa results along with extinction parameters measured for HD 62542 and HD 26947 see Table 2. Both HD 62542 and HD 29647 exhibit bumps with position and width parameters which lie outside the extreme limits found by Fitzpatrick amd Massa.

General reviews of the physical nature of the types of solid-state processes which might produce a bumplike feature are found in Gilra (1972) and Savage (1975). A number of factors can influence the position and width of an extinction bump if it arises from classical scattering and absorption by interstellar grains. Some of these factors include: (1) particle optical properties which change as the physical and thermal environment of the grains change; (2) particle size; (3) particle shape; (4) presence or absence of coatings or the existence of grain surfaces which have optical properties which differ from those of the grain interior. The sensitivity of the bump position to these factors depends on which of the many possible physical processes actually produces the bump.

In recent years, most of the theories for the production of the bump have focused on the process of plasma oscillations in small grains of carbon which are usually considered to be in the form of graphite. The sensitivity of the positions of extinction bumps to particle geometric properties is illustrated in Table 3 where we list the values of the central position of extinction bumps for a variety of particle sizes and shapes computed with classical Mie scattering theory and the bulk optical constants of graphite from Taft and Phillips (1965). As can be seen, a rather modest modification of the grain geometrical characteristics produces large changes in the position of the computed bump. Table 3 also lists the expected positions of extinction bumps produced by amorphous carbon and amorphous carbon annealed at 2200 C (see Hecht 1986). From these numbers we see that the degree of disorder in the solid-state form of matter in the absorbing solid also plays an important role in determining the solid's optical constants and hence bump position.

Various suggestions have been made to address the problem of the stability of the bump position. In the diffuse interstellar dust model of Mathis, Rumpl, and Nordsieck (1977, hereafter MRN) which employs a power-law size distribution, the bump is mostly produced by plasma oscillations in graphite particles in or near the Rayleigh limit. For such particles the position of the bump is relatively insensitive to changes in the particle sizes. According to MRN, the bulk optical properties of graphite as measured by different experimental groups exhibit large enough range so that spherical graphite particles in the small size limit may indeed have a bump centered near the average observed value of 2175 Å. An alternate solution has been advanced by Hecht (1986) who has considered the implications of the Fitzpatrick and Massa (1986) measurements. In

reviewing the many possibilities, Hecht concludes that the 2175 Å feature is caused by a population of small hydrogen-free carbon grains. He notes that large carbon grains (which will have lower temperatures than the small grains) will likely retain a surface layer of attached hydrogen atoms and that this coating will produce a substantial suppression of the bump. Hecht also proposes that the width of the bump, which changes considerably from one sight line to another, is probably influenced by temperature effects and size effects among the population of small (5 to 50 Å) hydrogen-free carbon grains which he believes causes the feature.

Within the framework of the Hecht model for the ultraviolet extinction bump, the weak bumps for HD 62542 and HD 26947 might be explained by environmental effects. In the dense interstellar environments for these two sight lines perhaps even the very small carbon grains have surface layers of hydrogen and therefore weakened bump strengths. The great breadth of the bumps would then have to be explained through size distribution and temperature effects. The shifted bump positions would also have to be explained by such effects.

While the discussion above seems reasonable, it is important to emphasize that a number of other effects may also be operating to modify the extinction bumps observed toward HD 62542 and HD 29647. Compositional differences, grain coagulation, grain shattering, or the growth of icy mantles are just a few of the many possibilities. The icy mantle suggestion was advanced by Snow and Seab (1980) to explain the anomalous ultraviolet extinction to HD 26947. A search for the 3.1 μm H_2O ice feature by Whittet *et al.* (1981) toward HD 26947 was unsuccessful, while a more sensitive observation by Goebel (1983) revealed an IR absorption feature near 3.1 μm with a strength of about 10%. Scattering and absorption calculations for graphite grains coated with crystalline H_2O ice predict that the resultant extinction bumps are weakened *and* shifted to longer wavelengths (Whittet *et al.* 1981). The weak bump for HD 26947, however, is shifted to shorter wavelengths. If the weak feature seen by Goebel actually is produced by H_2O ice absorption, the ice might therefore exist on another component of the interstellar dust. Thin H_2O ice coatings on small grains are expected to produce absorption edges near $\lambda^{-1} = 6.37\ \mu m^{-1}$ (Field, Partridge, and Sobel 1965; Whittet *et al.* 1981; Massa, Savage, and Fitzpatrick 1983). Such an ice edge having a strength of about 0.3 mag could exist in the extinction curve for HD 26947 shown in Figure 4. However, we note that the visibility of the UV H_2O ice edge will be sensitive to such variables as the distribution of sizes of the particles being coated as well as the distribution in sizes of the coatings themselves. Detailed model calculations will be required to evaluate the true implications of the undulations in the HD 29647 extinction curve for $\lambda^{-1} > 6\ \mu m^{-1}$.

Although H_2O ice coatings would be expected to shift the 2175 Å feature to longer wavelengths, it is possible to have other kinds of coatings which shift the feature to shorter wavelengths. Gilra (1972) discusses the effect coatings have on the position of plasma resonances such as those produced by graphite. In the small particle limit for spherical particles, the plasma resonance will occur between the wavelengths where $\epsilon_1(\lambda) = -2$ and $\epsilon_1(\lambda) = -2\,\epsilon_c(\lambda)$, where $\epsilon_1(\lambda)$ is the real part of the dielectric constant for the spherical particle being coated and $\epsilon_c(\lambda)$ is the real part of the dielectric constant for the coating material. In the case of plasma resonances in graphite, the feature will be shifted to longer wavelengths for $\epsilon_c > 1$ and to shorter wavelengths for $\epsilon_c < 1$. While H_2O ice has $\epsilon_c > 1$ in the wavelength region of interest, it is interesting that NH_3 ice has $\epsilon_c > 1$ for $\lambda > 2000$ Å but near 1990 Å the NH_3 absorption edge will cause ϵ_c to become less than 1 for λ slightly less than 1990 Å. The presence of this absorption edge near the bump position might actually create a broadening of the bump profile. Among other plausible coatings it is noteworthy that metals such as Fe have $\epsilon_c < 1$ in the relevant wavelength range.

One of the most intriguing aspects of the extinction bumps observed for HD 62542 and HD 29647 is that they more closely resemble the bumps expected for small spherical graphite particles than any of the bumps previously observed. Reference to Tables 2 and 3 shows that the "normal" observed bump with $\lambda_0 = 2175$ Å and $\gamma = 0.99\ \mu m^{-1}$ occurs at the wrong wavelength and with too narrow a width to be compatible with classical scattering by graphite having the bulk optical constants as measured by Taft and Phillips (1965). Of course, it is easy to imagine that graphite in the diffuse interstellar medium has somewhat different optical constants and

TABLE 3

SENSITIVITY OF EXTINCTION BUMP POSITIONS TO PARTICLE CHARACTERISTICS

Substance	Size (μm)[a]	Shape	$\lambda_0^{-1}(\mu m^{-1})$	λ_0(Å)	$\gamma(\mu m^{-1})$	Notes
Graphite	$r < 0.005$	Sphere	4.83	2070	1.19	1
Graphite	0.01	Sphere	4.76	2100	1.19	1
Graphite	0.02	Sphere	4.54	2200	1.26	1
Graphite	0.03	Sphere	4.35	2300	1.71	1
Graphite	0.04	Sphere	4.21	2375	2.62	1
Graphite	"Small"	Spheroidal (a/b = 2)	5.10	1960	1.19	1, 2
Graphite	"Small"	Spheroidal (a/b = 1.67)	5.00	2000	1.19	1, 2
Graphite	"Small"	Spheroidal (a/b = 1.0)	4.83	2070	1.19	1, 2
Graphite	"Small"	Spheroidal (a/b = 0.5)	4.54	2200	1.19	1, 2
Amorphous carbon	"Small"	Sphere	4.17	2400	...	3
Amorphous carbon annealed at 220 C	"Small"	Sphere	~4.55	~2200	...	3

[a] For particle size, "small" implies the particle is in the Rayleigh limit.

NOTES.—(1) Bulk optical constants for graphite have been taken from Taft and Phillips 1965. When optical constants from other investigators are used, the bump positions shift by about 100 Å (see MRN). (2) Spheroidal particles in the small size limit where *a* and *b* refer to the major and minor axis, respectively. The bump parameter values listed are from Wickramasinghe and Nandy 1974. (3) These values for the bump position are from Hecht 1986.

that those constants produce a bump for particles in the Rayleigh limit near the observed wavelength with the appropriate width. However, it is an interesting coincidence that the bumps toward HD 62542 and HD 29647 have positions and widths which are very compatible with the theoretical expectations for small bare spherical graphite particles in or near the Rayleigh limit. Perhaps the bumps we are measuring toward these two stars are "normal" for interstellar graphite grains and the so-called "normal" bumps for diffuse cloud matter are representative of interstellar graphite grains which have somehow become modified.

Finally we cannot rule out the interesting possibility that the bumps measured toward HD 62542 and HD 29647 reveal the underlying graphite component of the interstellar dust and that the bump seen at 2175 Å along diffuse cloud lines of sight is produced by some other process.

b) *The Far-Ultraviolet Extinction*

The extinction curves for HD 62542 and HD 29647 are very unusual in the FUV. In interpreting the significance of these curves, it is important to emphasize that the results given in Figures 3 and 4 are presented as extinction *normalized* to $E(B-V) = 1.0$. In such a normalized extinction curve, high FUV extinction might arise either from an enhancement of that small particle component responsible for the FUV extinction or by a reduction in the effectiveness of the particles responsible for extinction between the B and V photoelectric bands.

In the MRN interstellar dust model the FUV extinction is provided by intermediate-size graphite and small silicate grains. Thus an enhancement in the relative numbers of these grains compared to that component of the dust producing $E(B-V)$ extinction could explain an enhanced FUV extinction. Seab and Shull (1983) showed that an attractive theory for providing such an enhancement is shock processing of interstellar grains. To test this theory, Seab and Shull modeled the shock processing of an MRN dust mixture and found significant processing for shock speeds as low as 40 km s^{-1}. The calculation reveals that grain-grain collisions and nonthermal sputtering are the dominant destruction mechanisms and these processes destroy more large grains than small and destroy more silicates than graphite. The modeling reveals that the large silicate grains which mostly provide $B-V$ reddening are the most susceptible to destruction. The result of the shock processing of an MRN mixture according to Seab and Shull is therefore a reduction in the value of $E(B-V)$ for a given mass of dust which shows up as a strong 2175 Å bump and large far-UV extinction in extinction curves normalized to $E(B-V) = 1.0$. Unfortunately, the basic input physics required for carrying out the theory of shock processing of interstellar grains appears uncertain. Strazzulla, Barate, and Magazzu (1985) have criticized the Seab and Shull shock processing theory. By examining the laboratory studies of low-energy sputtering of solids, they conclude that graphite and silicate grains will be almost equally destroyed at shock velocities greater than 70 km s^{-1} and at lower velocities graphite is preferentially eroded. Until the theoretical predictions are clarified, it appears dangerous to try to interpret extinction curve variations based on theories of shock processing.

The FUV extinction toward HD 62542 is the highest so far found for a Milky Way star. The swept-up nature of the region certainly suggests that shock processing may have played a significant role in the early history of the dust which is now seen along the sight line to HD 62542. However, a number of other processes may also have occurred. A combination of shock processing followed up by the dust modifications which likely occur in dense interstellar environments as discussed in § VI*a* will probably be required to provide a complete understanding of the unusual extinction toward HD 62542.

The extinction curves for HD 62542 and HD 29647 go counter to the general trend of finding low FUV extinction curves for dust in dense interstellar environments (see Mathis 1987). In the case of HD 62542, the swept-up nature of the interstellar environment (see § V*a*) suggests that this may have occurred through shock processing of interstellar grains. However, in the case of HD 29647 such an explanation seems untenable since the local environment appears relatively undisturbed (see § V*b*). In this latter case, a more plausible explanation is that grain growth through mantles or coagulation has reduced the $(B-V)$ reddening efficiency of those grains which mostly contribute to visual extinction but has left the far-ultraviolet extinction relatively unchanged with the result that the far-ultraviolet extinction appears enhanced in an $E(B-V)$ *normalized* extinction curve. The idea of icy coatings is consistent with the 3.1 μm H_2O ice feature observations of Goebel (1983). Mantles which consist of ices of abundant species such as H_2O, NH_3, or CH_4 can reveal their presence through their strong UV absorption edges near $\lambda^{-1} = 6.37$, 5.03, and 7.41 μm^{-1}, respectively (Field, Partridge, and Sobel 1965) and weak ($\Delta m = 0.3$ mag) edges near these positions could certainly exist in the observed curve for HD 26947. The sensitivity of the expected appearance of these absorption edges to assumed particle and coating parameters is demonstrated in the theoretical curves shown by Field, Partridge, and Sobel (1965).

The highly anomalous character of the UV extinction bump toward HD 62542 and HD 26947 suggests another possibility for the unusual FUV extinction. Graphitic carbon exhibits a second plasma resonance which in the small particle limit peaks in absorption at about 800 Å. Perhaps the physical effect which has altered the wavelength and breadth of the 2175 Å feature has produced a major modification in the character of this second resonance such that the effects of this modification are visible in the FUV region accessible to the *IUE*.

c) *General Extinction Considerations for Stars in Dense Interstellar Environments*

The two UV extinction curves found for HD 62542 and HD 26947 should cause major concern about the validity of using an average extinction curve to correct UV energy distributions for the presence of interstellar dust. It has been common in recent years to assume that extinction curves with low FUV extinction (e.g., Orion-like or ρ Oph–like) are generally applicable in dense environments. The curves for HD 62542 and HD 26947 reveal that there are cases where the extinction has the opposite behavior. The extreme nature of the curve for HD 62542 unfortunately reveals that the errors associated with using a standard curve can be enormous. For example, if a curve like that for θ ^{1}C Ori (Bohlin and Savage 1981) is assumed to be valid but the actual curve is like that seen toward HD 62542 and if the standard process of "ironing out" the bump is followed then the corrected fluxes at 1250 Å compared to the V band would be in error by an astonishing 11 mag for $E(B-V) = 1.0$.

In addition to the standard problem of correcting astronomical observations for the presence of dust, there are important physical processes which are strongly affected by the dust properties. For example, interstellar chemical processes are

influenced by the transfer of dissociating FUV radiation into dense interstellar regions. The exceedingly high FUV extinction found toward HD 62542 will likely play a major role in influencing the chemistry in the cloud toward this interesting star. Also, the presence of large numbers of small grains along this sight line may substantially modify the grain surface chemistry over that found in normal diffuse clouds. Follow-up high-dispersion *IUE* and ground-based observations of narrow interstellar absorption lines in the spectrum of HD 62542 may therefore be exceedingly interesting.

We acknowledge valuable discussions with J. Mathis regarding UV extinction and the theories of interstellar dust. D. Leckrone provided helpful suggestions regarding the UV energy distributions of B stars having peculiar abundances. Marilyn Meade provided assistance with the *IUE* data handling. We thank the *IUE* observatory staff for their help in acquiring and processing the satellite data. The final data reductions were processed at the Midwest Regional Astronomical Data Analysis Facility in Madison. This work was supported through NASA grants NAG-186 and NAG-832.

REFERENCES

Abbott, D. C., Bieging, J. H., Churchwell, E., and Torres, A. V. 1986, *Ap. J.*, **303**, 239.
Beuermann, K. P. 1973, *Ap. Space Sci.*, **20**, 27.
Bohlin, R. C., and Savage, B. D. 1981, *Ap. J.*, **249**, 109.
Bohlin, R. C., Holm, A. V., Savage, B. D., Snijders, M. A. J., and Sparks, W. M. 1980, *Astr. Ap.*, **85**, 1.
Bohren, C. F., and Huffman, D. R. 1983, *Absorption and Scattering of Light by Small Particles*, (New York: Wiley-Interscience), Chap. 12.
Brandt, J. C., Stecher, T. P., Crawford, D. L., and Maran, S. P. 1971, *Ap. J. (Letters)*, **163**, L99.
Cameron, R. C. 1966, *Georgetown Obs. Monogr.*, No. 21.
Cardelli, J. A., and Wallerstein, G. 1986, *Ap. J.*, **302**, 492.
Cassatella, A., and Lloyd, C. 1987, *IUE/ESA Newsletter*, No. 27, p. 13.
Chanot, A., and Sivan, J. P. 1983, *Astr. Ap.*, **121**, 19.
Clavel, J., Gilmozzi, R., and Prieto, A. 1986, *IUE/ESA Newsletter*, No. 26, p. 65.
Clayton, G. C., and Fitzpatrick, E. L. 1987, *A.J.*, **92**, 157.
Cousins, A. W. J., and Stoy, R. H. 1962, *Royal Obs. Bull.*, No. 64
Cousins, A. W. J., Eggen, O. J., and Stoy, R. H. 1961, *Royal Obs. Bull.*, No. 25.
Cowley, A., Cowley, C., Jaschek, M., and Jaschek, C. 1969, *A.J.*, **74**, 375.
Crutcher, R. M. 1985, *Ap. J.*, **288**, 604.
Eggen, O. J. 1969, *Roy. Obs. Bull.*, No. 137.
Elias, J. H. 1978, *Ap. J.*, **224**, 857.
Elitzur, M., and Watson, W. D. 1978, *Ap. J. (Letters)*, **222**, L141.
———. 1980, *Ap. J.*, **236**, 172.
Feast, M. L., Thackeray, A. D., and Wesselink, A. J. 1955, *Mem. R.A.S.*, **67**, 51.
Federman, S. R. 1982, *Ap. J.*, **257**, 125.
Field, G. B., Partridge, R. B., and Sobel, H. 1965, in *Interstellar Grains*, ed J. M. Greenberg and T. P. Roark (NASA SP-140), p. 207.
FitzGerald, M. P. 1970, *Astr. Ap.*, **4**, 234.
Fitzpatrick, E. L. 1986, *A.J.*, **92**, 1068.
Fitzpatrick, E. L., and Massa, D. 1986, *Ap. J.*, **307**, 286.
Gilra, D. P. 1972, in *Scientific Results from the OAO 2*, ed. A. D. Code (NASA SP-310), p. 295.
Goebel, J. H. 1983, *Ap. J. (Letters)*, **268**, L41.
Gott, J. R., and Ostriker, J. P. 1971, in *The Gum Nebula and Related Problems*, ed. S. P. Maran, J. C. Brandt, and Y. P. Stecher. (NASA SP-332), p. 42.
Greenstein, J. L. 1981, *Ap. J.*, **245**, 124.
Harris, A. W., and Cassatella, A. 1985, *IUE/ESA Newsletter*, No. 22, p. 9.
Hecht, J. H. 1986, *Ap. J.*, **305**, 817.
Hecht, J. H., Holm, A. V., Donn, B., and Wu, C.-C. 1984, *Ap. J.*, **280**, 228.
Hecht, J., and Nuth, J. 1982, *Ap. J. (Letters)*, **258**, L78.
Herbig, G. H. 1975, *Ap. J.*, **196**, 129.
Hua, C.-T., Woo, J.-O., and Nguyen, H.-D. 1983, *Astr. Ap. Suppl.*, **53**, 407.
Jacoby, G. H., Hunter, D. A., and Christian, C. A. 1984, *Ap. J. Suppl.*, **56**, 257.
Jaschek, M., Jaschek, C., Grenier, S., Gomex, A. E., and Heck, A. 1980, *Astr. Ap.*, **81**, 142.
Johnson, H. L. 1966, *Comm. Lunar Planetary Obs.*, **4**, 99.
Johnson, H. L., and Iriarte, B. 1958, *Lowell Obs. Bull.*, **4**, 47.
Koorneff, J., and Code, A. D. 1981, *Ap. J.*, **247**, 860.
Kurucz, R. L. 1979, *Ap. J. Suppl.*, **40**, 1.
Leckrone, D. S. 1973, *Ap. J.*, **185**, 577.
Lesh, J. R. 1968, *Ap. J. Suppl.*, **17**, 371.
Massa, D., and Fitzpatrick, E. L. 1986, *Ap. J. Suppl.*, **60**, 305.
Massa, D., Savage, B. D., and Fitzpatrick, E. L. 1983, *Ap. J.*, **266**, 662.
Mathis, J. S. 1987, in *Scientific Acomplishments of the IUE*, ed. Y. Kondo *et al.* (Dordrecht: Reidel), p. 517.
Mathis, J. S., Rumpl, W., and Nordsieck, K. H. 1977, *Ap. J.*, **217**, 425 (MRN).
Meyers, K. A., Snow, T. P., Federman, S. R., and Breger, M. 1985, *Ap. J.*, **288**, 148.
Nandy, K., Thompson, G. I., Jamar, C., Monfils, A., and Wilson, R. 1976, *Astr. Ap.*, **52**, 63.
Olson, G. L., and Castor, J. I. 1981, *Ap. J.*, **244**, 79.
Panek, R. J., and Savage, B. D. 1976, *Ap. J.*, **206**, 167.
Prevot, M. L., Lequeux, E., Maurice, L., Prevot, L., and Rocca-Volmerange, B. 1984, *Astr. Ap.*, **132**, 389.
Reynolds, R. J. 1976*a*, *Ap. J.*, **203**, 151.
———. 1976*b*, *Ap. J.*, **206**, 679.
Savage, B. D. 1975, *Ap. J.*, **199**, 92.
Savage, B. D., Massa, D., Meade, M. R., and Wesselius, P. R. 1985, *Ap. J. Suppl.*, **59**, 397.
Savage, B. D., and Mathis, J. S. 1979, *Ann. Rev. Astr. Ap.*, **17**, 73.
Seab, C. G., and Shull, J. M. 1983, *Ap. J.*, **275**, 652.
Seaton, M. J. 1979, *M.N.R.A.S.*, **187**, 73P.
Sitko, M. L., Savage, B. D., and Meade, M. R. 1981, *Ap. J.*, **246**, 161.
Sivan, J. P. 1974, *Astr. Ap. Suppl.*, **16**, 163.
Snow, T. P., and Seab, C. G. 1980, *Ap. J. (Letters)*, **242**, L83.
Straizys, V., Cernis, K., and Hayes, D. S. 1985, *Ap. Space Sci.*, **112**, 251.
Straizys, V., Wisniewski, W. Z., and Lebofsky, M. J. 1982, *Ap. Space Sci.*, **85**, 271.
Strazzulla, G., Baratta, G. A., and Magazzu, A. 1985, *Astr. Express*, **1:4-6**, 143.
Taft, E. A., and Phillips, H. R. 1965, *Phys. Rev.*, **138**, A197.
van der Hucht, K. A., Cassinelli, J. P., and Williams, P. M. 1986, *Astr. Ap.*, **168**, 111.
Wallerstein, G., Silk, J., and Jenkins, E. B. 1980, *Ap. J.*, **240**, 834.
Weaver, R., McCray, R., Castor, J., Shapiro, P., and Moore, R. 1977, *Ap. J.*, **218**, 377.
Whittet, D. C. B., Bode, M. F., Evans, A., and Butchart, I. 1981, *M.N.R.A.S.*, **196**, 81P.
Wickramasinghe, N. C., and Nandy, K. 1974, *Ap. Space Sci.*, **26**, 123.
Woolf, S. C. 1983, *The A-Stars: Problems and Perspectives* (NASA SP-463), p. 144.
Woolf, S. C. 1967, *Ap. J. Suppl.*, **15**, 21.
Wu, C.-C., *et al.* 1983, *IUE Ultraviolet Spectral Atlas, IUE/NASA Newsletter*, No. 22.

JASON A. CARDELLI and BLAIR D. SAVAGE: Department of Astronomy, University of Wisconsin, 475 N. Charter St. Madison, WI 53706